frontiers | Frontiers in Physics

TYPE Original Research
PUBLISHED 11 February 2025
DOI 10.3389/fphy.2025.1518626

OPEN ACCESS

EDITED BY
Alan Wuosmaa,
University of Connecticut, United States

REVIEWED BY
Angela Bonaccorso,
National Institute of Nuclear Physics of Pisa, Italy
Alberto Camaiani,
Dipartimento di Fisica e Astronomia, Italy

*CORRESPONDENCE
Valdir Guimarães,
valdirg@if.usp.br

RECEIVED 28 October 2024
ACCEPTED 07 January 2025
PUBLISHED 11 February 2025

CITATION
Guimarães V, Nistal PC, Olorunfunmi SD, Linares R and Lubian J (2025) Distance of interaction: a phenomenological analysis of elastic scattering data induced by light projectiles.
Front. Phys. 13:1518626.
doi: 10.3389/fphy.2025.1518626

Distance of interaction: a phenomenological analysis of elastic scattering data induced by light projectiles

Valdir Guimarães[1]*, Pierre Camilo Nistal[1], Sunday D. Olorunfunmi[1,2], Roberto Linares[3] and Jesus Lubian[3]

[1]Instituto de Física, Universidade de São Paulo, São Paulo, Brazil, [2]Department of Physics and Engineering Physics, Obafemi Awolowo University, Ile-Ife, Nigeria, [3]Instituto de Física, Universidade Federal Fluminense, Niterói, Rio de Janeiro, Brazil

Introduction: A phenomenological analysis, based on distances, has been performed for elastic scattering data induced by tightly bound (^{11}B, ^{12}C, and ^{16}O), weakly bound (^{6}Li, ^{7}Li, ^{7}Be, and ^{9}Be), and exotic (^{6}He, ^{8}B, ^{11}Be, and ^{15}C) nuclei on light (^{27}Al), medium (^{58}Ni and ^{120}Sn), and heavy mass (^{208}Pb) targets, respectively, at energies close to the Coulomb barrier.

Methods: The cross-section data on the angular distributions have been converted as a function of the distance of the closest approach.

Results: From a fitting analysis, critical interaction and strong absorption distances were extracted from the data.

Discussion: Correlation was observed with the projectile cluster configuration for the data on the target ^{208}Pb.

KEYWORDS

nuclear reactions, nuclear structures, elastic scattering, critical interaction distance, heavy ions

1 Introduction

The complexity of nuclear structure and reactions is governed by the interplay of the strong and electroweak interactions. The need to understand how these forces act within the atomic nucleus drives experimental and theoretical efforts to explore the limits of nuclear existence. Today, 288 isotopes are known to be stable or long-lived nuclei in a vast landscape that may encompass nearly 7,800 nuclei, according to theoretical models [1, 2]. Some of these nuclei are tightly bound in their ground state and have been well-described as spherical in shape, such as ^{16}O, ^{58}Ni, and ^{208}Pb. Other nuclei, on the other hand, are weakly bound and can exhibit clustering signatures, such as ^{7}Li ($\alpha + t$) and ^{9}Be ($\alpha + \alpha + n$). There are also neutron- and proton-rich nuclei near the boundaries of the driplines with even more exotic configurations. Nuclei such as ^{8}B (^{7}Be+p) and ^{11}Be ^{10}Be+n) have shown an exotic configuration, in which the valence nucleon orbits a core at a large distance. Others, such as ^{11}Li (^{9}Li+$n + n$), have two valence-orbiting nucleons, forming a structure that resembles Borromean rings and are, therefore, referred to as Borromean nuclei.

Due to the large extended distance of nuclear matter, ^{11}Li is considered a halo nucleus, while ^{6}He is called a skin nucleus. The structure of halo in the nucleus can be considered

TABLE 1 List of selected energies of the angular distributions with the ^{27}Al target considered in this work.

Projectile	Energies (MeV)	Ref.
^{6}He	9.5, 11.0, 12.0, and 13.4	[30]
^{6}Li	7.0, 8.0, and 10.0	[31]
^{7}Li	7.0, 8.0, 9.0, and 10.0	[32]
^{7}Be	15.2 and 15.4	[33]
^{9}Be	12.0 and 14.0	[34]
^{8}B	15.3 and 21.7	[35]
^{11}B	24.0, 36.0, and 48.0	[36]
^{12}C	21.0	[37]
^{14}N	52.3	[38]
^{16}O	28.0	[37]

a threshold effect, arising from the small separation energy of the one- or two-valence nucleons. In a halo structure, the valence nucleon(s) is (are) nearly decoupled from a well-defined inert core. Such a structure makes halo nuclei a suitable object to explore the behavior of open quantum systems (OQS) since the valence particle in a halo nucleus is sensitive to any interaction with continuum states and the external environment. In this case, the valence neutrons would tunnel the potential well with a slowly decaying exponential tail extending beyond the range of the potential. Thus, neutron halo can be considered one of the most exotic phenomena of the quantum tunneling effect of a loosely bound system, which can be considered to be an OQS. The boundary for defining a nucleus as halo is not exactly clear, and there are some other nuclei that are also considered to have a halo structure, such as ^{11}Be and ^{15}C. For the proton-rich nuclei, the situation is even less defined since the Coulomb barrier between the core and the valence proton prevents it from having the same behavior as neutron valence. The radial density distribution deduced for elastic scattering of ^{8}B + p exhibited a clear halo structure with the root-mean-square (rms) matter radius R_m = 2.58 (6) fm and the rms halo radius R_h = 4.24 (25) fm [3]. This result, combined with the large breakup cross sections [4] and the narrow longitudinal momentum distribution for the ^{7}Be core [5], is very strong experimental evidence of a proton-halo structure in ^{8}B nuclei. Despite the lack of experimental evidence, some other proton-halo candidates are ^{12}N (S_p = 0.601 MeV) [6] and ^{17}Ne (S_{2p} = 0.933 MeV) [7, 8]. In summary, several exciting phenomena have emerged from the investigations of the structures of these light nuclei, and several other phenomena remain to be investigated. In particular, whether and/or why halo and cluster structures in light nuclei occur preferentially at thresholds, which is a clear characteristic of OQS, is an actual topic under investigation.

Nuclear reaction is one of the most commonly employed techniques for exploring the structures exhibited by nuclei across the vast nuclear landscape. To extract structure information on the colliding partners, reliable reaction models and high-quality experimental data are required. In this regard, elastic scattering is the simplest and most studied process among the possible outcomes in collisions between two nuclei. From the analysis of these elastic scattering angular distributions, we can obtain information on both the static (deformation and cluster configuration) and dynamic (couplings to nonelastic reaction channels) effects on the collision. The theoretical description of this process is often based on quantum theories with a model space of the reaction channels. Some of the ingredients in these calculations are the effective optical potential between the projectile and target nuclei, coupling constants, and the structure of the nuclei involved. The shape of the optical potential is usually linked to the overall geometry of the nuclei. By choosing specific targets, it is possible to focus on the properties of the projectile. For example, the peculiar cluster configurations in some light exotic nuclei, such as ^{6}He, ^{8}B, ^{11}Be, and ^{15}C, induce a strong coupling to the continuum states. In turn, this coupling introduces a characteristic dynamic polarization (attractive or repulsive) in the optical potential that is not present in the elastic scattering induced by strongly bound projectiles. A review investigating the elastic scattering data can be found in [9, 10]. A specific review on the elastic scattering of light radioactive projectiles can be found in [11], where the peculiar surface properties (static effects) of exotic weakly bound nuclei are highlighted. The strong coupling effect in elastic scattering has been reviewed and well-discussed in [12].

Although a quantum formulation for elastic scattering is well-grounded on a theoretical basis, adopting a semi-classical approach is useful for complementary phenomenological analysis. In classical mechanics, scattering is described in terms of trajectories and connects the distance of the closest approach D to the asymptotic scattering angle. Therefore, the angular distribution of normalized elastic cross sections can be converted to normalized cross sections as a function of distance D. Under this transformation, it is possible to determine the strong absorption (D_s) and the interaction distances (D_i) for a binary collision. The former corresponds to the distance at which the ratio of elastic scattering to Rutherford scattering ($d\sigma/d\sigma_{Ruth}$) drops to 0.25. The corresponding angle at which $d\sigma/d\sigma_{Ruth}$ = 0.25 is also called the grazing angle (θ_{gr}) or the quarter-point angle ($\theta_{1/4}$). The distance of strong absorption is closely related to the radius of the stable nucleus, as discussed in [13, 14]. However, the nuclear radius is not as easily defined for weakly bound and exotic nuclei, which can have an exotic cluster structure and/or a very diffuse density distribution at the surface region. The interaction distance represents the distance at which the nuclear potential (or a long-range Coulomb interaction) starts manifesting itself during the income trajectory in the nuclear collision and the cross-section ratio starts to deviate from unity. In the present work, the critical interaction distance is defined when the elastic cross-section ratio to Rutherford, $d\sigma/d\sigma_{\mathrm{Ruth}}$, is equal to 0.98. This value corresponds to the S-matrix's absolute value of 0.99, and it is the distance where the flux from elastic scattering starts to be absorbed.

In this work, we present a semiclassical phenomenological analysis based on distances to investigate static and dynamic

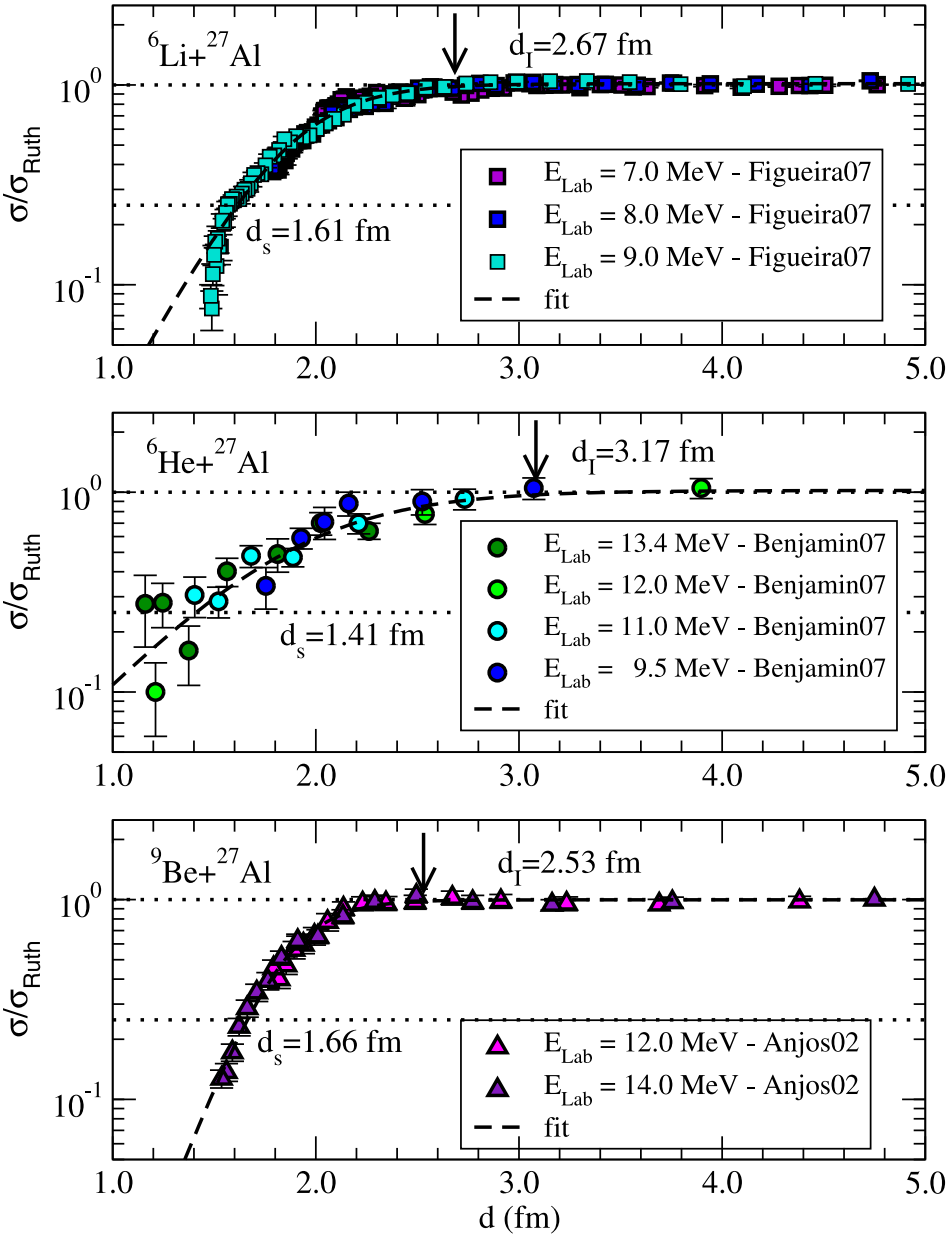

FIGURE 1
σ/σ_{Ruth} as a function of the reduced distance for ^{6}Li, ^{6}He, and ^{9}Be + ^{27}Al systems at the indicated energies. The cross-section data are from references indicated in Table 1.

effects on the elastic scattering of light nuclei, at energies close to the Coulomb barrier. We present new results for the analysis of elastic scattering data on the targets ^{27}Al and ^{120}Sn, which can be considered a sequel of the previous analysis on the targets ^{58}Ni [15] and ^{208}Pb [16]. On account of this, this analysis was inspired by the initial work of Pakou and Rusek, which is presented in [17]. Systematic analysis, in which several data sets can be compared on the same grounds, has been shown to be a powerful tool for investigating general behavior and highlighting the particular properties of some of the nuclei involved.

2 Critical distance of interaction

The cross sections of the angular distributions, listed in Tables 1, 3, were converted from the angular dependence to the distance of the closest approach on a Rutherford trajectory and then to reduced distances. In classical scattering, the distance at the closest approach is related to the incident energy and scattering angle in the center of mass (c.m.) frame as follows:

$$D = \frac{1}{2}\left[k\frac{Z_p Z_t}{E_{c.m.}}\right]\left[1+\frac{1}{\sin(\theta/2)}\right], \quad (1)$$

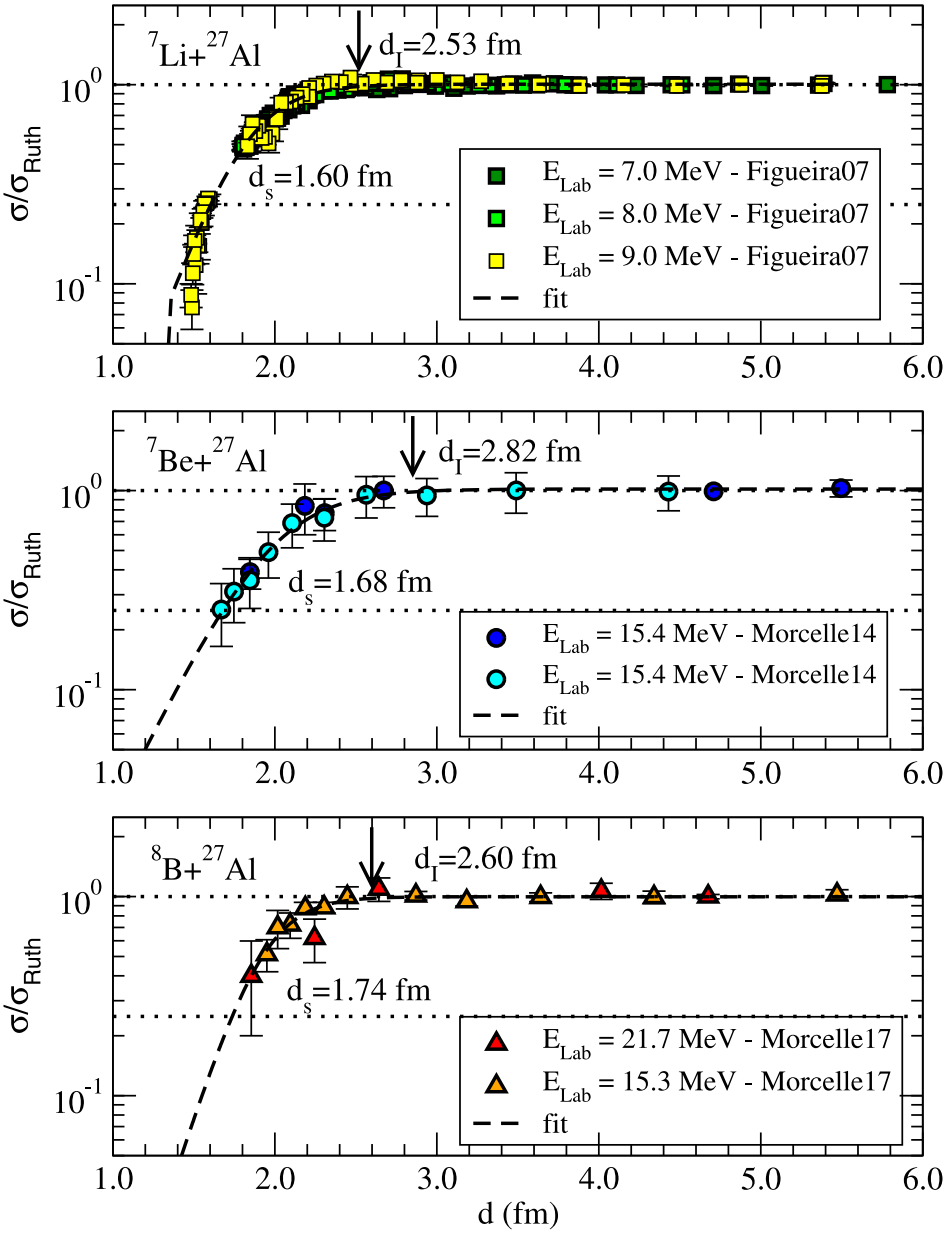

FIGURE 2
σ/σ_{Ruth} as a function of the reduced distance for ^{7}Li, ^{7}Be, and ^{8}B+ ^{27}Al systems at the indicated energies. The cross-section data are from references indicated in Table 1.

with $k = 1.44$ MeV.fm. Z_i and A_i correspond to the atomic number and mass of the nuclei of the projectile ($i = p$) and the target ($i = t$), respectively. For a better comparison of the different data sets, involving different projectiles, we consider the reduced distance at the closest approach (d) defined as follows:

$$d = \frac{D}{A_p^{1/3} + A_t^{1/3}}. \quad (2)$$

By plotting the data as a function of d, we can combine several data sets corresponding to the angular distribution $d\sigma/d\sigma_{\mathrm{Ruth}}$ *versus* $\theta_{\mathrm{c.m.}}$ measured in different energies into one data set $d\sigma/d\sigma_{\mathrm{Ruth}}$ *versus* d. This is very convenient for elastic angular distributions with radioactive projectiles, where cross sections are usually obtained at fewer angles for each energy but at several different energies.

After converting all the angular distributions to the reduced distance dependence, we observed a common behavior among them. The $d\sigma/d\sigma_{\mathrm{Ruth}}$ ratio for all systems is very close to unity for large distances and begins to decrease rapidly at short distances. The cross sections are dropped because of strong absorption of the elastic flux into nonelastic channels, mostly fusion for very small distances. In the intermediate region, the static (cluster structure) and dynamic (couplings) effects play a relevant role for the tightly, weakly bound, and exotic

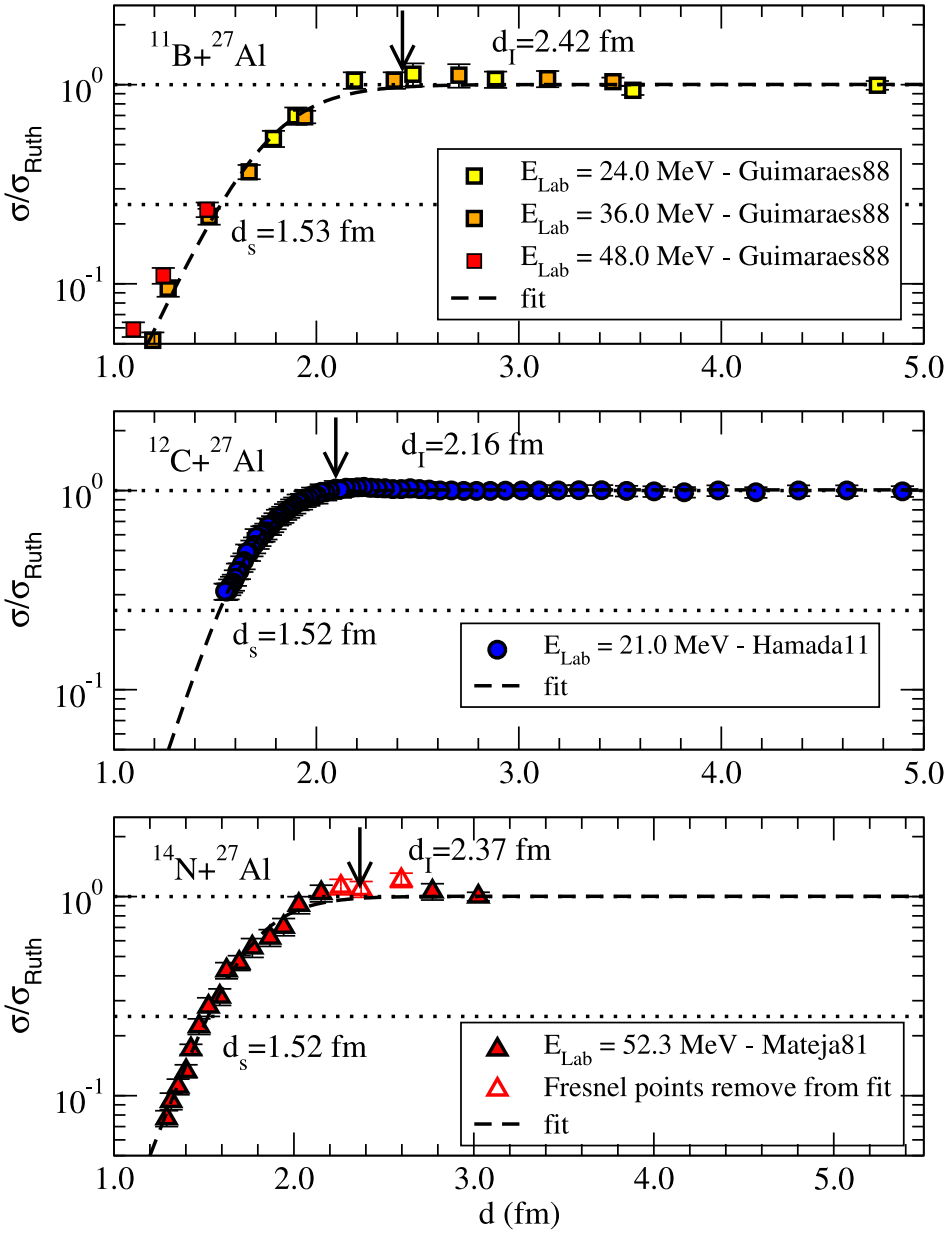

FIGURE 3
σ/σ_{Ruth} as a function of the reduced distance for ^{11}B, ^{12}C, and ^{14}N + ^{27}Al systems at the indicated energies. The cross-section data are from references indicated in Table 1.

configuration projectile, which can be related to the reduced distance of strong absorption d_s and the reduced distance of critical interaction d_i. As mentioned above, the reduced critical interaction distance is defined as the distance for which the ratio $d\sigma/d\sigma_{\mathrm{Ruth}}$ drops to 0.98, while the reduced strong absorption distance (also associated with the grazing angle or with $\theta_{1/4}$) is defined for when $d\sigma/d\sigma_{\mathrm{Ruth}}$ is 0.25. We can extract these distances from the plots of the angular distributions as a function of the reduced distance of the closest approach. The procedure of the present work is also performed in [15, 16], which defines a phenomenological expression that could describe the region where the cross sections fall. The adopted expression is based on a Boltzmann exponential function and is defined as follows:

$$y = \frac{p_1}{\left[1 + e^{-p_2(d-p_3)}\right]}, \tag{3}$$

where $y \equiv d\sigma/d\sigma_{\mathrm{Ruth}}$. The parameters p_1, p_2, and p_3 are free to vary during the data fitting process. The expression itself has no physical meaning and can only be used in the restricted region of the cross-section ratio between 1 and 0.1. The parameter p_1 is related to the asymptotic value of y for a large distance d,

TABLE 2 Distances of interaction for ^{27}Al determined from σ/σ_{Ruth} as a function of the reduced distance. S_n corresponds to the separation energy of the nucleus for the given cluster structure.

Projectile	S_n (MeV)	config	d_i (fm)	d_s (fm)	p_1	p_2 (fm^{-1})	p_3 (fm)	χ^2_{red}
^{6}He	0.973	α+2n	3.17 (23)	1.410 (22)	1.021 (93)	−2.45 (35)	1.870 (97)	1.2
^{6}Li	1.474	α+d	2.67 (8)	1.614 (12)	1.013 (1)	−4.23 (3)	1.878 (2)	4.3
^{7}Li	2.467	α+t	2.53 (8)	1.604 (12)	1.007 (1)	−5.14 (4)	1.820 (2)	3.7
^{7}Be	1.587	α+^{3}He	2.82 (7)	1.683 (14)	1.018 ()	−3.83 (10)	1.972 (51)	0.06
^{8}B	0.137	^{7}Be+p	2.60 (11)	1.736 (10)	0.998 (20)	−5.9 (16)	1.923 (53)	0.48
^{9}Be	1.665	^{8}Be+n	2.53 (18)	1.660 (9)	0.992 (5)	−6.71 (11)	1.832 (7)	0.57
^{11}B	8.689	^{7}Li+α	2.41 (7)	1.529 (10)	1.011 (25)	−5.10 (12)	1.746 (18)	5.5
^{12}C	7.366	^{8}Be+α	2.16 (5)	1.520 (8)	1.009 (18)	−7.31 (42)	1.674 (7)	0.09
^{14}N	7.551	^{13}C+p	2.37 (8)	1.523 (9)	1.003 (41)	−5.72 (29)	1.715 (21)	1.05

TABLE 3 List of selected energies of the angular distributions with the ^{120}Sn target considered in this work.

Projectile	Energies (MeV)	Reference.
^{6}He	17.4, 18.05, 19.8, and 20.5	[39]
	22.2	[40]
^{6}Li	44.0	[41]
	22.8	[42]
^{7}Li	20, 22, 24, and 26	[43]
^{8}B	38.7 and 46.1	[4]
^{9}Be	26.0, 27.0, and 28.0	[24]
^{10}B	31.5, 33.5, and 35.0	[25]
	37.5	[44]
^{11}Be	32.0	[23]
^{11}B	32.6, 34.7, and 37.2	[45]
^{12}C	60.0	[46]
^{16}O	53.0, 54.0, and 55.0	[47]
	55.0 and 65.75	[48]

and thus, it is associated with the normalization of the data. When its value is very close to unity, it indicates a suitable normalization of the data. The whole procedure is very reliable in obtaining the values of the reduced critical interaction and strong absorption distances, in particular for the data at energies close to the Coulomb barrier with no strong Fresnel peak. The errors in the values of the parameters were also obtained and are related to the quality of the cross-section data. This work mainly aims to obtain a reduced critical interaction and strong absorption distances for different projectile types such as exotic, weakly and strongly bound, stable, and radioactive light nuclei on light, medium, and heavy mass targets. Furthermore, the idea is to verify the correlation between these distances and, for instance, the projectile cluster configuration or the separation energies for the given cluster configuration. To perform a systematic and comparative analysis, we consider the reduced distances, where the size and geometric effect of the projectiles associated with mass dependence are somehow disregarded. The remaining geometric effect is associated only with the projectile deformation, cluster, and halo configurations.

3 Data analysis

We have surveyed the literature for a series of measured angular distributions of elastic scattering involving tightly bound (^{10}B, ^{11}B, ^{12}C, ^{13}C, and ^{14}N), weakly bound (^{6}Li, ^{7}Li, ^{7}Be, and ^{9}Be), and exotic (^{6}He, ^{8}B, ^{11}Be, and ^{15}C) nuclei projectiles on ^{27}Al, ^{58}Ni, ^{120}Sn, and ^{208}Pb targets, at energies close to the Coulomb barrier. In addition to the new analysis of elastic scattering on ^{27}Al and ^{120}Sn targets, we included, in the present work, part of the results of the previous analysis on ^{58}Ni and ^{208}Pb targets [15, 16] and the new analysis of data recently published for ^{8}B [18], ^{10}C [19], ^{13}C [20], and ^{15}C [21] projectiles on ^{208}Pb target, which is not present in the previous work. The targets considered here are among the most common ones used in elastic scattering measurements, mainly because they are tightly bound and not very deformed, and even double magic as in the case of ^{208}Pb target, for which we expected to have very low collectivity or influence of other channels in the elastic (except for the ^{27}Al target, which may have some collective effect). Thus, the dynamic and static effects on the elastic process can mostly rely on the projectile's properties.

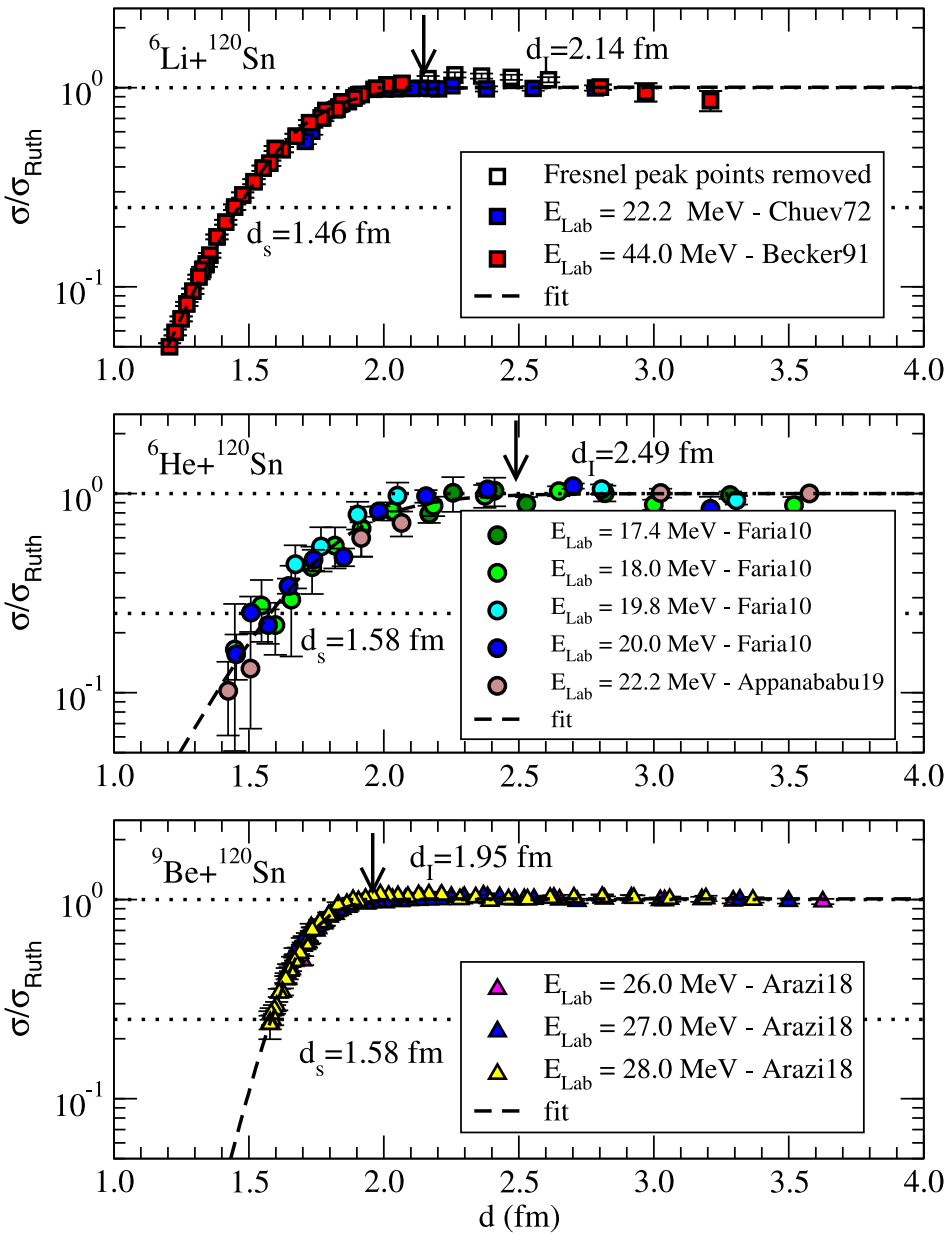

FIGURE 4
σ/σ_{Ruth} as a function of the reduced distance for ^{6}Li, ^{6}He, and ^{9}Be + ^{120}Sn systems at the indicated energies. The cross-section data are from references indicated in Table 1.

The data used in the present analysis are compiled in Tables 1, 3. We have only selected elastic scattering data for light projectiles on ^{27}Al, ^{58}Ni, ^{120}Sn, and ^{208}Pb targets, at energies around the Coulomb barrier. This allows us to explore the collisions mediated by a nuclear interaction, with the ^{27}Al target, all the way through the Coulomb-dominated interaction, with ^{208}Pb and the (possible) nuclear Coulomb interferences with the ^{58}Ni and ^{120}Sn targets. For some systems, the angular distributions have also been measured at several other energies well above the Coulomb barrier. Still, we selected the angular distributions measured close to the Coulomb barrier, where the Fresnel peak is absent or very small.

3.1 Distances for light mass target A = 27

The selected angular distributions and their corresponding energies and references used in the analysis of elastic scattering on the light ^{27}Al target are listed in Table 1, which includes data induced by tightly bound (^{11}B, ^{12}C, ^{14}N, and ^{16}O), weakly bound (^{6}Li, ^{7}Li, ^{7}Be, and ^{9}Be), and exotic (Borromean ^{6}He and proton-halo ^{8}B) projectiles. The data for the elastic scattering were, actually, extracted from the EXFOR database (https://www-nds.iaea.org/exfor/) [22] and converted to a function of the reduced distance of the closest approach, according to Equations 1, 2. The plots of the cross sections

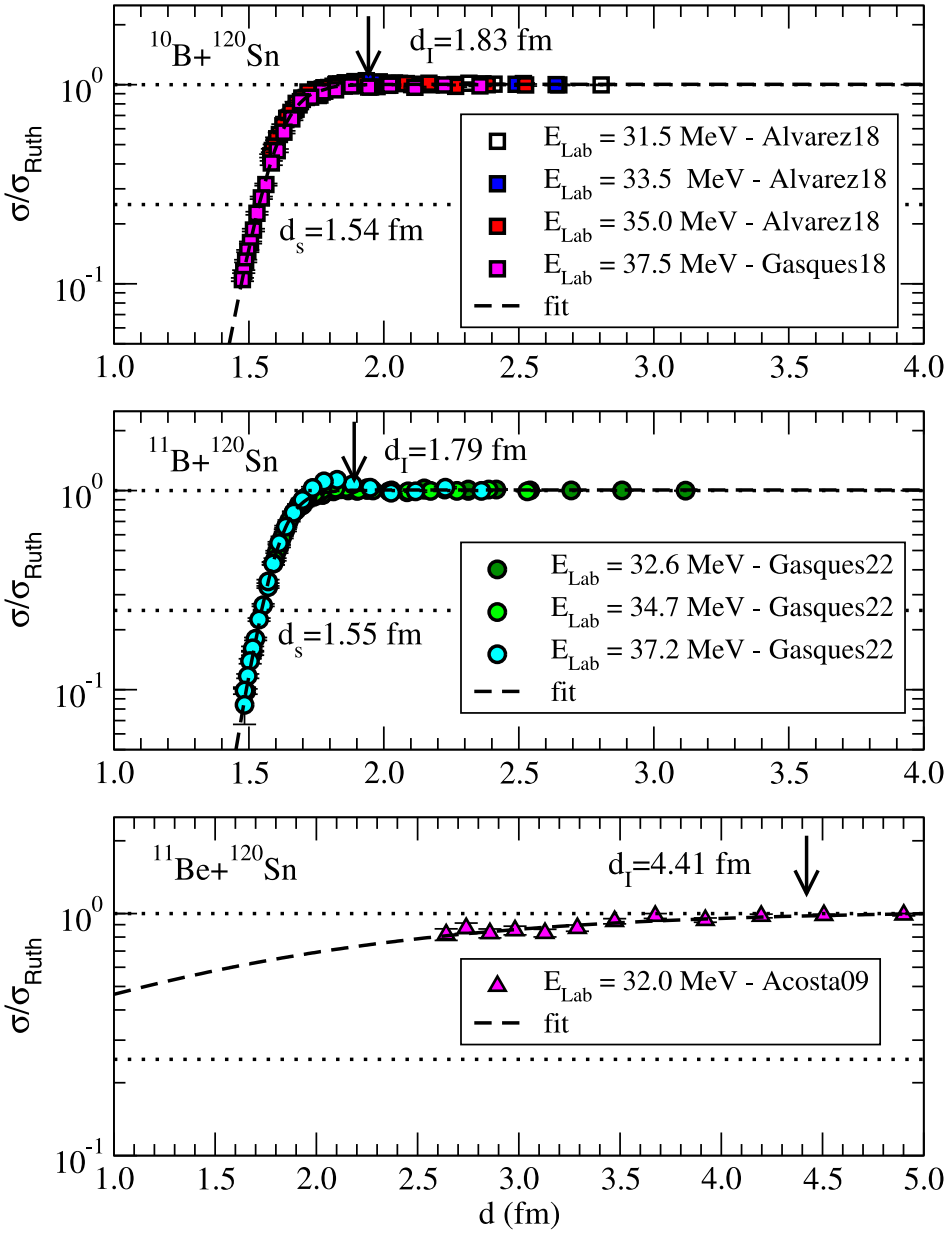

FIGURE 5
σ/σ_{Ruth} as a function of the reduced distance for ^{10}B, ^{11}B, and ^{11}Be + ^{120}Sn systems at the indicated energies. The cross-section data are from references indicated in Table 1.

versus distances for ^{6}Li, ^{6}He, ^{9}Be, ^{6}Li, ^{7}Li, ^{7}Be, ^{8}B, ^{11}B, ^{12}C, and ^{14}N are shown in Figures 1–3. The results of the fitting using Equation 3 and the corresponding parameters obtained are listed in Table 2. It is worth highlighting the good quality of the data for elastic scattering induced by ^{7}Li, ^{9}Be, and ^{12}C projectiles. However, some angular distributions have a clear normalization issue. For the present analysis, correct normalization of the angular distributions is important since the critical interaction distance is defined on the basis of it. For example, the cross-section ratios for the angular distribution for ^{11}B + ^{27}Al at E_{Lab} = 24.0 MeV and ^{12}C + ^{27}Al at E_{Lab} = 21.0 MeV were re-normalized by a factor of 0.95 and 0.98, respectively, so at large distances, the ratios become, on average, equal to 1.0. For the ^{8}B and ^{7}Be + ^{27}Al systems, the error bars for the first two points were artificially reduced to 1% to ensure that the parameters p_1 were obtained close to unity. For the ^{14}N + ^{27}Al system, the Fresnel points, indicated as open symbols in the plot, were removed from the fitting. χ^2_{red} obtained for the fit is also listed in the Table 2. As can be seen, χ^2_{red} obtained for the ^{7}Be + ^{27}Al system is very small due to the large error bars in the cross sections, while for ^{12}C + ^{27}Al, it is small due to the small fluctuation of the data compared to the error bars.

As the results of the fit, the reduced critical interaction distance, d_i, and the reduced strong absorption distance, d_s, could be extracted and are listed in Table 2. The uncertainties in the reduced

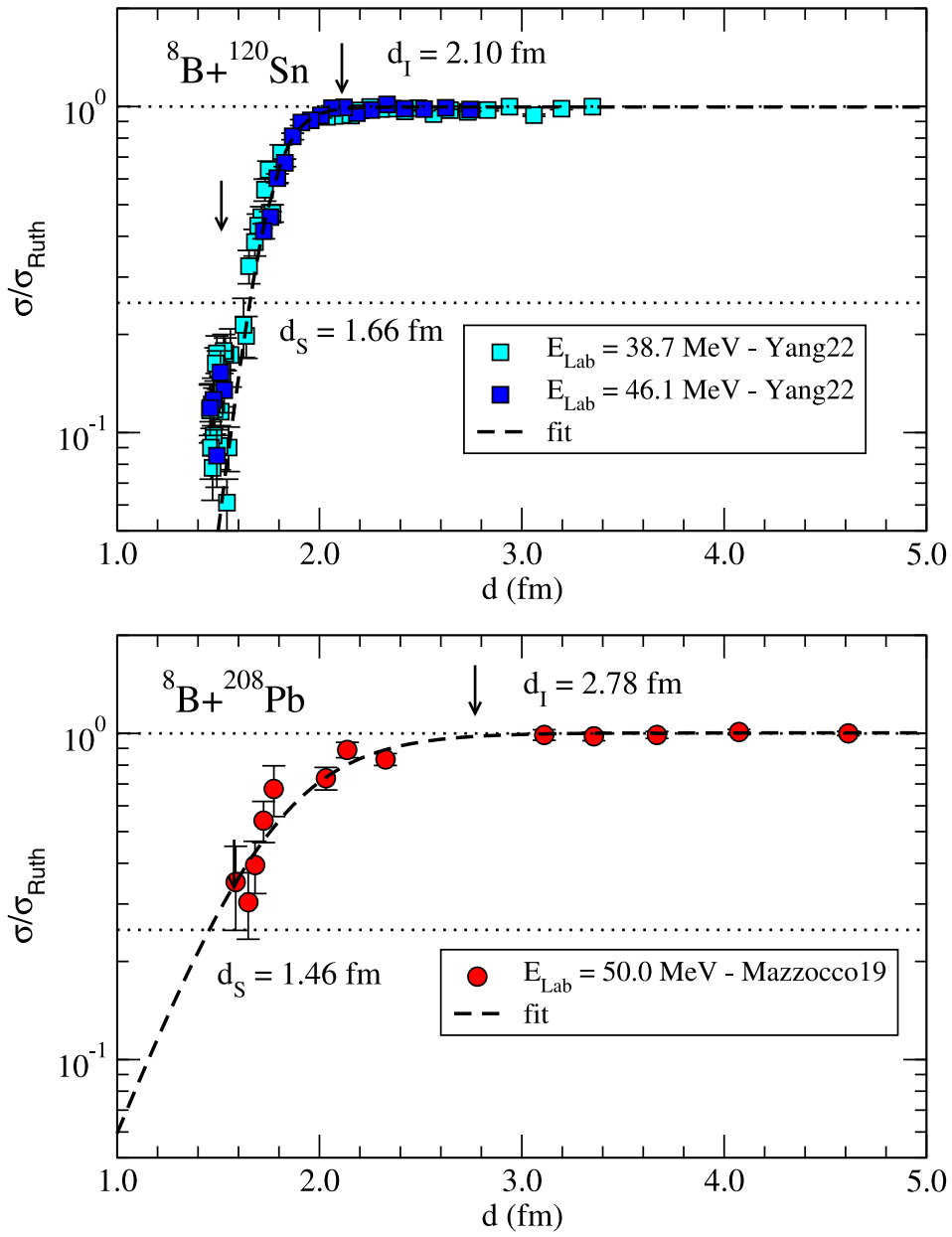

FIGURE 6
σ/σ_{Ruth} as a function of the reduced distance for ^{8}B + ^{120}Sn and ^{8}B + ^{208}Pb systems at the indicated energies. The cross-section data are from references indicated in Table 1.

critical interaction and strong absorption distances were obtained, considering the difference in the distance for the cross-section ratios 0.97–0.99 and 0.24–0.26, respectively. The quality and fluctuation of the data are indirectly included in these uncertainties by the fitting curve. Inspecting the reduced distances listed in Table 2, we can conclude that the average reduced strong absorption distances for the system with exotic and weakly bound projectiles are d_s = 1.62(8) fm, a little larger than for the tightly bound projectile, d_s = 1.526(4) fm. For the reduced critical interaction distance, the values are d_i = 2.72(18) fm and d_i = 2.31(10) fm for the two groups, respectively. Although the difference is not large, it is not negligible. The highest value is obtained for the ^{6}He + ^{27}Al system, due to the exotic configuration of the ^{6}He projectile. The small fluctuation among the values of the critical interaction distances might be due to the fact that the long-range Coulomb interaction, which can be quite different for different projectile types, is weak for this light target.

3.2 Distances for medium-mass target A = 58

The phenomenological distance analysis has already been performed for the elastic scattering data induced by some light nuclei as ^{6}He, ^{6,7,8}Li, ^{7,9,10,11}Be, ^{8,10,11,12}B, ^{9,11}Li, ^{12}C, and ^{16}O, on

TABLE 4 Distances of interactions for ^{120}Sn determined from σ/σ_{Ruth} as a function of the reduced distance. S_n corresponds to the separation energy of the nucleus for the given cluster configuration.

Projectile	S_n(MeV)	config	d_i (fm)	d_s (fm)	p_1	p_2 (fm^{-1})	p_3 (fm)	χ^2_{red}
^{6}He	0.973	α+2n	2.49 (10)	1.579 (10)	0.999 (5)	−5.51 (39)	1.778 (13)	1.12
^{6}Li	1.474	α+d	2.14 (6)	1.461 (8)	1.005 (8)	−7.03 (6)	1.618 (3)	4.41
^{7}Li	2.467	α+t	1.95 (3)	1.566 (6)	1.007 (1)	−12.16 (8)	1.657 (1)	4.20
^{8}B	0.137	^{7}Be+p	2.10 (6)	1.656 (4)	0.996 (1)	−11.76 (14)	1.749 (2)	9.79
^{9}Be	1.665	^{8}Be+n	1.95 (3)	1.582 (5)	1.014 (4)	−12.23 (26)	1.674 (1)	0.80
^{10}B	4.461	^{6}Li+α	1.83 (3)	1.538 (5)	1.004 (1)	−16.65 (8)	1.604 (1)	4.55
^{11}B	8.664	^{7}Li+α	1.79 (2)	1.547 (2)	1.007 (1)	−19.35 (10)	1.605 (1)	7.87
^{11}Be	0.502	^{10}Be+n	4.45 (10)	—-	1.055 (4)	−7.68 (3)	1.06 (53)	1.26
^{12}C	7.366	^{8}Be+α	1.82 (2)	1.536 (4)	1.017 (35)	−14.38 (6)	1.612 (6)	162
^{16}O	7.162	^{12}C+α	1.72 (2)	1.528 (3)	1.000 (1)	−27.00 (15)	1.568 (3)	19.0

the medium-mass targets ^{58}Ni and ^{64}Zn, reported in [15]. Since this analysis has already been published, we are just resuming the import results. The values of the reduced interaction distance can be divided into three groups. The average value for systems with weakly bound projectiles ^{6,7,8}Li and ^{7,9}Be is d_i = 2.18(49) fm; for the tightly bound system, the average value is d_i = 1.87(1) fm, while for the exotic projectiles, ^{6}He, ^{8}B, and ^{11}Be, the reduced critical distances are much larger, being in the range of d_i = 2.5 to 3.0 fm. The differences in the values between these three groups are more pronounced than for light ^{27}Al, indicating stronger dynamic effects since static effects are related to the projectile itself. The extended matter density (static effect) and the lower breakup threshold (dynamic effect) of the exotic projectiles induce the nuclear forces to be felt beyond the classical range, resulting in a strong absorption and early deviation of the dσ/d$\sigma_{\rm Ruth}$ ratio from unity. In particular, the extension of the direct interaction region for the ^{6}He and ^{11}Be projectiles is closely related to the importance of long-range Coulomb and/or nuclear interaction for these exotic projectiles. This effect also provokes a strong damping of the Fresnel diffraction peak observed in the corresponding angular distributions compared to those for the tightly bound isotopes of the same elements (^{4}He and ^{10}Be).

3.3 Distances for the medium-mass target A = 120

The selected data used in the analysis of elastic scattering on the medium-mass ^{120}Sn target are listed in Table 3. For this target, we also analyzed the elastic scattering data for systems including tightly bound (^{11}B, ^{12}C, and ^{16}O), weakly bound (^{6}Li, ^{7}Li, and ^{9}Be), and exotic (Borromean ^{6}He, proton-halo ^{8}B, and neutron-halo ^{11}Be) projectiles. Furthermore, for this target, the elastic scattering cross-section data were extracted from the EXFOR database (https://www-nds.iaea.org/exfor/) [22] for most of the system and converted to a function of the reduced distance of the closest approach. The corresponding plots of the cross-section ratios *versus* distances for ^{6}Li, ^{6}He, ^{9}Be, ^{10}B, ^{11}B, ^{11}Be, and ^{8}B are shown in Figures 4–6. The parameters and corresponding values of χ^2_{red}, obtained as the result of the fitting using Equation 3, are listed in Table 4. The data for this target are of much better quality than those for the aluminum target. In particular, we can highlight the good quality of the data for ^{9}Be, ^{10}B, and ^{11}B, obtained in recent years at the Tandar Laboratory in Argentina [23, 24, 25]. By removing data points at the Fresnel peak for the ^{11}B + ^{120}Sn system, the values for the distances did not change, but χ^2_{red} drops from 7.87 to 3.00. The good quality for the ^{9}Be + ^{120}Sn system is also reflected in the small χ^2_{red} = 0.80. For the ^{12}C + ^{120}Sn data, the obtained large χ^2_{red} value is due to the too small error bars reported in EXFOR.

For this target, the average reduced strong absorption distance for the tightly bound projectiles is d_s = 1.537(6) fm, which is consistent with the value obtained for the ^{27}Al target. For exotic and weakly bound projectiles, the distance is d_s = 1.57(4) fm, which is again just a little larger than that for tightly bound projectiles. For the reduced critical interaction distance, the averaged values are d_i = 1.80(4) fm for tightly bound projectiles and d_i = 2.13(4) fm for exotic and weakly bound projectiles. The distance obtained for ^{11}Be was not included in the previous averaging. The ^{11}Be projectile is a neutron-rich isotope that forms a halo configuration with the ^{10}Be core and a weakly bound neutron (S_n = 504(6) keV). The quite large value for the critical interaction distance, d_i = 4.41(7) fm, for the ^{11}Be + ^{120}Sn system is clear experimental evidence of the strong effect of the ^{11}Be neutron halo structure on elastic scattering, at energies close to the Coulomb barrier. This large absorption effect has already been observed for the elastic scattering of ^{11}Be on the ^{64}Zn target [26] close to the barrier energy and also on the ^{208}Pb

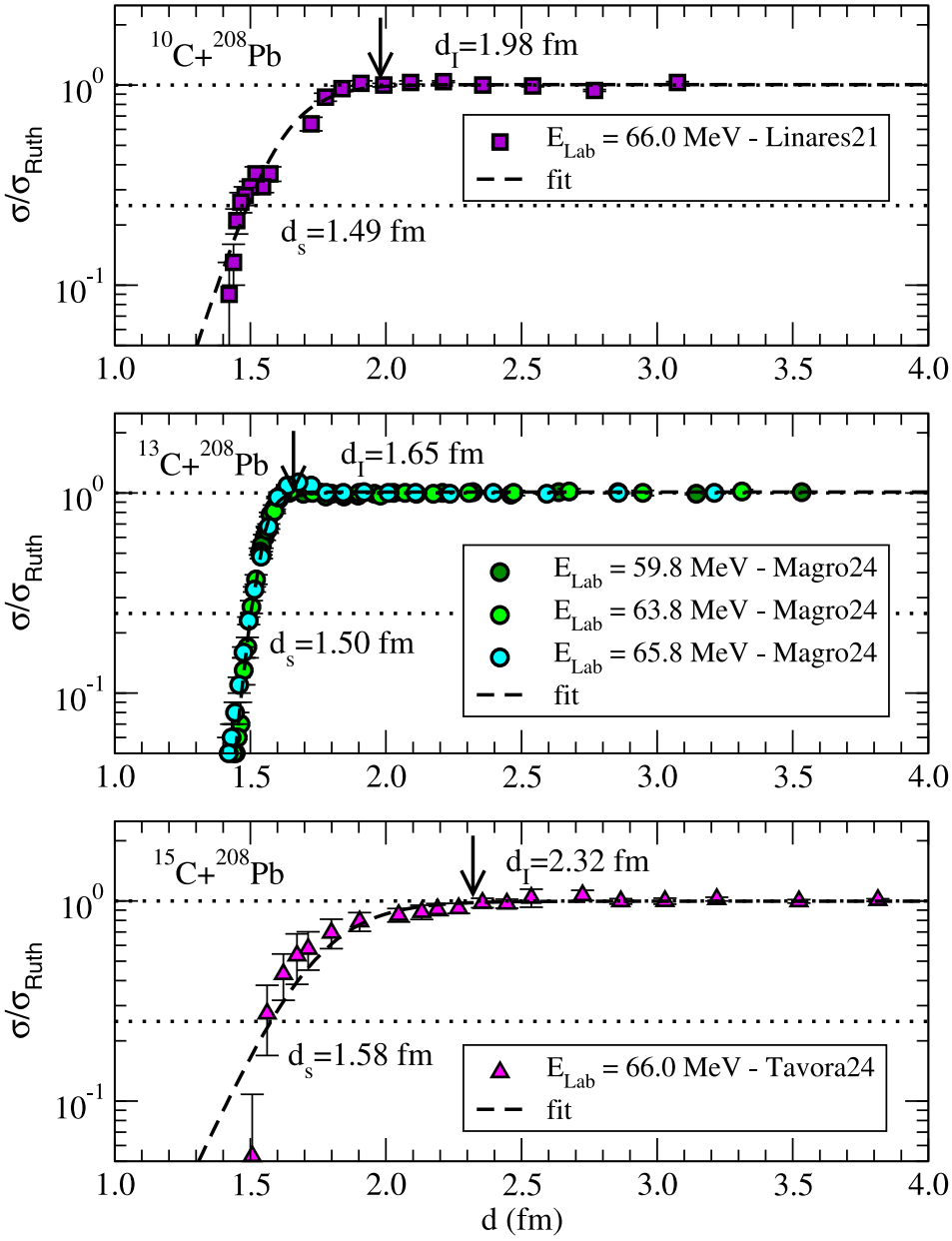

FIGURE 7
σ/σ_{Ruth} as a function of the reduced distance for ^{10}C, ^{13}C, and ^{15}C + ^{208}Pb systems at the indicated energies. The cross-section data are from references indicated in Table 1.

target at higher energies (three times the Coulomb barrier) [27]. The strong absorption in elastic scattering induced by this projectile is due to the strong influence of the break-up channel, related to its loosely bound structure. By comparison, this effect is not as drastic for the proton-rich halo nucleus ^{8}B, with proton separation energy S_p = 0.138 MeV for the ^{7}Be+p configuration, indicated by the not-so-large reduced critical distance of interaction for this nucleus, d_i = 2.10(6) fm, shown in Figure 6. The other large critical interaction distance is obtained for the ^{6}He projectile, d_i = 2.49(7) fm. Both ^{6}He (α+n+n) and ^{9}Be (α+α+n) nuclei are considered to have a Borromean configuration, where by removing one of the elements, the other two also dissociate, resembling the Borromean ring. However, ^{6}He is radioactive and weakly bound (S_{2n} = 0.973 MeV), while ^{9}Be is a stable bound nucleus with S_n = 1.665 MeV. The difference in their critical interaction distances can be attributed to static and dynamic effects related to the extended matter distribution and the lower breakup threshold, respectively. The extended critical interaction distance for neutron-rich ^{6}He and ^{11}Be projectiles is again clear experimental evidence of the importance of a long-range Coulomb and/or nuclear interaction for these exotic projectiles. Consequently, these give rise to a combination of effects of a large value of Coulomb dipole polarizability

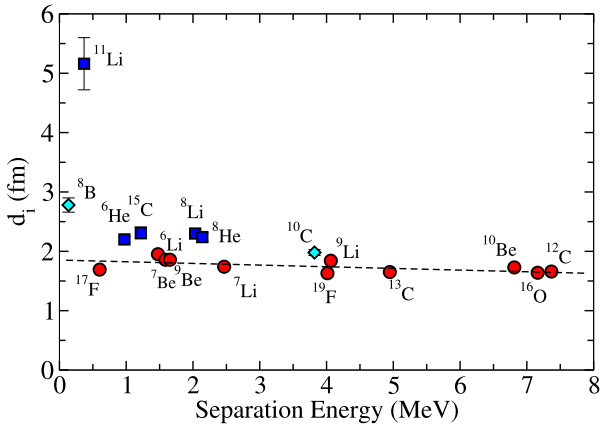

FIGURE 8
Reduced critical distance of interaction as a function of the separation energy for the nuclei indicated. The dashed curve corresponds to the trend of the data for the weakly and tightly bound nuclei in red. The plot is an upgrade of this figure in [16].

and large transfer breakup probabilities already observed experimentally.

3.4 Distances for heavy-mass target A = 208

The present phenomenological distance analysis has already been performed for the elastic scattering data induced by some light nuclei such as ^{6}He, ^{6}Li, ^{7}Li, ^{7}Be, ^{8}He, ^{8}Li, ^{8}B ^{9}Li, ^{9}Be, ^{10}Be, ^{11}Li, ^{12}C, ^{16}O, ^{17}F, and ^{19}F on the ^{208}Pb target, reported in [16]. The analysis of the heavy spherical target yielded interesting results related to the dependence of the cluster configuration throughout the separation energy and the critical distance of interaction. By choosing heavy targets with a stronger Coulomb field, all absorption effects can be related to the projectile configuration. We are now expanding the analysis with data recently published on ^{8}B, ^{10}C, ^{13}C, and ^{15}C. The plots for the cross-section ratio as a function of the reduced distances for these nuclei are shown in Figures 6, 7. In particular, we emphasize the importance of the new data for proton-rich nuclei that were not included in the previous analysis. The low binding energy for ^{8}B projectile ($S_p = 0.138$ MeV) and the nuclear proton-halo configuration (^{7}Be+p) contribute to the opening of several elastic absorption channels, observed as a large total reaction cross section [18]. In addition, because of the low binding energy, the projectile can easily break up near the target Coulomb and nuclear fields, enhancing the breakup channel, mainly at energies close to the Coulomb barrier. However, since the proton is in the p orbital, the matter density is not as extended far from the core due to the centrifugal barrier. The critical interaction distance obtained for this projectile is $d_i = 2.78(4)$ fm, which is the second largest in the table, just below that for ^{11}Li. The large distance of interaction is not due to the extended matter density (static effect) but due to the lower breakup threshold and stronger coupling to the continuum. The other proton-rich nucleus is ^{10}C. It has a α+α+p+p configuration, and it is called the Brunnian or super Borromean nucleus [28]. This configuration is similar to that for ^{10}Be (α+α+n+n). However, the presence of the neutrons makes ^{10}Be a quite tightly bound nucleus. As noted in [19, 29], the exotic cluster configuration for ^{10}C induces strong absorption, making the critical interaction distance for this nucleus similar to the weakly bound nuclei.

The critical distance of interaction obtained for the new data on ^{8}B, ^{10}C, ^{13}C, and ^{15}C projectiles were included in the systematic as a function of the separation energy, as performed in [16]. The extended and upgraded plot can be seen in Figure 8. The values used in this plot are listed in Table 5 in the column for ^{208}Pb. The proton halo ^{8}B has the second-largest critical distance of interaction. The neutron halo ^{15}C also has a considerable critical interaction distance. On the other hand, ^{10}C and ^{13}C follow the trend of the weakly and tightly bound nuclei; the weaker the projectile, the more significant the critical interaction distance.

4 Comparative analysis

A comparative analysis was also performed by combining all the distances obtained for exotic, weakly bound, and tightly bound projectiles on light (^{27}Al), medium (^{58}Ni and ^{120}Sn), and heavy (^{208}Pb) targets together. The values for all obtained strong absorption and critical interaction distances are listed in Tables 5, 6. A more complete set of data was obtained for ^{208}Pb since several elastic scattering experiments have been performed on this target, including the most recent for ^{8}B, ^{10}C, ^{13}C, and ^{15}C. This makes the comparative analysis more reliable for this target, as shown in the previous section. We can observe in these tables that, although there are some fluctuations in the values for some projectiles, the average value for a reduced strong absorption distance is about the same for all targets analyzed here. As mentioned above, this distance is related somehow to the geometry (radius) of the nucleus. However, we should emphasize that what is obtained are the reduction distances, where a factor $1/(A_p^{1/3}+A_t^{1/3})$ has been applied. Therefore, the strong absorption distance (not the reduced one) should be larger for a larger mass target. This can be confirmed just by multiplying each of the average values, only by the target contribution of the reduction factor ($A_t^{1/3}$). In this case, the average values turn out to be $< 4.77 >$, $< 5.85 >$, $< 7.64 >$, and $< 9.02 >$ fm, for ^{27}Al, ^{58}Ni, ^{120}Sn, and ^{208}Pb targets, respectively. As expected, larger values are obtained for the larger-mass target. The reduced critical interaction distances should be larger than the corresponding reduced strong absorption distances. This is expected since not only static but also dynamic effects play a role in the elastic scattering process at distances larger than the strong absorption distance. However, as observed in the tables, the reduced critical interaction distances are smaller for heavier targets. The average values (taking the anomalous value for ^{11}Li) decrease for heavier targets. Again, this is the effect of the reduction factor (mass influences). The projectiles begin to feel the interaction at shorter distances for the lighter target. The average values after recovering the contribution of the target mass factor become $< 7.68 >$, $< 8.44 >$, $< 9.80 >$, and $< 11.56 >$ fm, for the targets ^{27}Al, ^{58}Ni, ^{120}Sn, and ^{208}Pb, respectively. We can conclude that more relevant information is obtained when a comparison is performed for different projectile types but on the same target.

TABLE 5 Distance of critical interaction for ^{27}Al, ^{58}Ni, ^{120}Sn, and ^{208}Pb.

Projectile	S_n(MeV)	^{27}Al	^{58}Ni	^{120}Sn	^{208}Pb
^{6}He	0.973	3.17 (23)	2.93 (13)	2.49 (10)	2.20 (5)
^{6}Li	1.474	2.67 (8)	2.22 (6)	2.14 (6)	1.95 (4)
^{7}Li	2.467	2.53 (8)	2.19 (5)	1.95 (3)	1.74 (2)
^{7}Be	1.587	2.82 (7)	2.17 (6)		1.86 (5)
^{8}He	2.140				2.24 (7)
^{8}Li	2.140		2.23 (3)		2.30 (7)
^{8}B	0.138	2.60 (11)	2.50 (10)	2.10 (6)	2.78 (12)
^{9}Li	4.064				1.84 (2)
^{9}Be	1.665	2.53 (18)	2.12 (6)	1.95 (3)	1.86 (2)
^{10}Be	6.812				1.73 (2)
^{1o}C	3.821		2.56 (16)		1.98 (5)
^{11}Li	0.369				5.16 (44)
^{11}B	8.664	2.41 (7)	1.88 (3)	1.79 (2)	1.75 (2)
^{12}C	7.366	2.16 (50)	1.83 (3)	1.84 (2)	1.66 (2)
^{13}C	4.946				1.65 (1)
^{15}C	1.218				2.32 (10)
^{16}O	7.162	2.13 (5)	1.80 (2)	1.72 (2)	1.64 (1)
		< 2.56(23) >	< 2.22(25) >	< 2.00(18) >	< 1.96(25) >

5 Summary

A semiclassical approach, by plotting the ratio of elastic cross section to the Rutherford value as a function of the distance of the closest approach on a Rutherford trajectory, was performed for some light projectiles on light (^{27}Al), medium (^{58}Ni and ^{120}Sn), and heavy (^{208}Pb) targets. This analysis is of special advantage for investigating angular distributions induced by low-statistics radioactive nuclei because several angular distributions can be grouped in one data set. In this sense, the present analysis is a good approach to check the quality of the data. The reduced critical and strong absorption distances obtained were compared, and the influence of static and dynamic effects on the elastic scattering process was discussed. Although these distances can be somehow related to the size of the nuclei, they are also influenced by the reaction mechanisms. In particular, the critical interaction distance has some correlation with the separation energy of the valence particles or a particular cluster configuration, which may affect the strength of the couplings and the importance of a particular channel. The significantly higher value obtained for exotic nuclei such as ^{11}Li, ^{6}He, ^{8}B, and ^{15}C can be understood as a result of the influence of the large Coulomb dipole polarizability of these projectiles, which induces a higher breakup probability. For a neutron-halo projectile, the Coulomb breakup originates only from the recoil of its core. However, for a proton-halo projectile, the valence proton also feels the effect of the direct Coulomb interaction with the Coulomb field of the target. Therefore, for a proton-halo projectile, the breakup will originate from a combination of three forces: the nuclear interaction with the target, the effective force due to the recoil of the core, and the direct proton–target Coulomb repulsion. The interplay between these three interaction modes is important in describing the angular distribution of the elastic scattering with proton-halo projectiles. These forces act coherently, and their final effects are due to strong interferences at the scattering angles, where the three forces have comparable values. An interesting discussion on the different behavior of the proton and neutron halo projectile in a reaction is presented in [49, 50]. In the present analysis, only the overall effects are observed as a large distance of interaction and, as also observed, are strongly related to the target mass. For the ^{208}Pb target, the extended and upgraded plot of the critical distance of interaction versus the separation energy for the given cluster configuration indicates a clear correlation.

TABLE 6 Distance of strong absorption for ^{27}Al, ^{58}Ni, ^{120}Sn, and ^{208}Pb.

Projectile	S_n(MeV)	^{27}Al	^{58}Ni	^{120}Sn	^{208}Pb
^{6}He	0.973	1.410 (22)	1.522 (15)	1.579 (10)	1.589 (7)
^{6}Li	1.474	1.614 (12)	1.600 (07)	1.461 (08)	1.521 (5)
^{7}Li	2.467	1.604 (10)	1.582 (07)	1.566 (06)	1.491 (3)
^{7}Be	1.587	1.683 (14)	1.603 (06)		1.509 (4)
^{8}He	2.140				1.718 (6)
^{8}Li	2.140		1.433 (10)		1.521 (5)
^{8}B	0.137	1.736 (10)	1.625 (10)	1.656 (04)	1.456 (15)
^{9}Be	1.665	1.660 (09)	1.480 (07)	1.582 (05)	1.540 (4)
^{10}Be	6.812				1.521 (2)
^{1}°C	3.821		1.412 (12)		1.491 (6)
^{11}Li	0.369				1.59 (4)
^{11}B	8.644	1,529 (10)	1.587 (04)	1.547 (02)	1.478 (3)
^{12}C	7.366	1.520 (08)	1.570 (03)	1.535 (04)	1.491 (2)
^{13}C	4.946				1.502 (2)
^{15}C	1.218				1.576 (8)
^{16}O	7.162	1.582 (15)	1.572 (02)	1.528 (03)	1.498 (2)
		< 1.59(7) >	< 1.54(6) >	< 1.56(4) >	< 1.53(4) >

Data availability statement

Publicly available datasets were analyzed in this study. These data can be found here: the original data are in the published paper already referred.

Author contributions

VG: conceptualization, data curation, formal analysis, funding acquisition, investigation, methodology, project administration, resources, software, supervision, validation, visualization, writing–original draft, and writing–review and editing. PN: formal analysis, investigation, and writing–review and editing. SO: data curation, formal analysis, investigation, and writing–review and editing. RL: formal analysis, investigation, validation, visualization, writing–original draft, and writing–review and editing. JL: investigation, validation, visualization, and writing–review and editing.

Funding

The author(s) declare that financial support was received for the research, authorship, and/or publication of this article. The authors acknowledge financial support from the Brazilian Funding Agencies: CNPq (Grant 303769/2021-1), FAPESP (Grants 2016/17612-7, 2022/14052-1 and 2024/02463-2), and INCT-FNA (Instituto Nacional de Ciência e Tecnologia-Física Nuclear e Aplicações) Proc. No. 464898/2014-5 and FAPERJ Proc. No. 210805/2024.

Conflict of interest

The authors declare that the research was conducted in the absence of any commercial or financial relationships that could be construed as a potential conflict of interest.

The author(s) declared that they were an editorial board member of Frontiers, at the time of submission.

This had no impact on the peer review process and the final decision.

Generative AI statement

The author(s) declare that no Generative AI was used in the creation of this manuscript.

Publisher's note

References

1. Erler J, Birge N, Kortelainen M, Nazarewicz W, Olsen E, Perhac AM, et al. The limits of the nuclear landscape. *Nature* (2012) 486:509–12. doi:10.1038/nature11188

2. Neufcourt L, Cao Y, Giuliani SA, Nazarewicz W, Olsen E, Tarasov OB. Quantified limits of the nuclear landscape. *Phys Rev C* (2020) 101:044307. doi:10.1103/PhysRevC.101.044307

3. Korolev GA, Dobrovolsky AV, Inglessi AG, Alkhazov GD, Egelhof P, Estradé A, et al. Halo structure of ^{8}B determined from intermediate energy proton elastic scattering in inverse kinematics. *Phys Lett B* (2018) 780:200–4. doi:10.1016/j.physletb.2018.03.013

4. Yang L, Lin C, Yamaguchi H, Moro AM, Ma NR, Wang DX, et al. Breakup of the proton halo nucleus 8b near barrier energies. *Nat Commun* (2022) 13:7193. doi:10.1038/s41467-022-34767-8

5. Kelley JH, Austin SM, Azhari A, Bazin D, Brown JA, Esbensen H, et al. Study of the breakup reaction ^{8}B→7Be+p; Absorption effects and E2 strength. *Phys Rev Lett* (1996) 77:5020–3. doi:10.1103/physrevlett.77.5020

6. Magro PLD, Guimaraes V, Linares R, et al. Elastic scattering in the ^{12}N+^{197}Au system at elab = 70 MeV. *Phys Rev C* (2025).

7. Lehr C, Wamers F, Aksouh F, Yu A, Álvarez-Pol H, Atar L, et al. Unveiling the two-proton halo character of ^{17}Ne: exclusive measurement of quasi-free proton-knockout reactions. *Phys Lett B* (2022) 136957:136957. doi:10.1016/j.physletb.2022.136957

8. Kanungo R, Chiba M, Adhiraki S, et al. Possibility of a two-proton halo in ^{17}Ne. *Phys Lett* (2003) 21:571. doi:10.1016/j.physletb.2003.07.050

9. Canto L, Guimarães V, Lubián J, Hussein M. The total reaction cross section of heavy-ion reactions induced by stable and unstable exotic beams: the low-energy regime. *Eur Phys J A* (2020) 281:281. doi:10.1140/epja/s10050-020-00277-8

10. Canto L, Gomes P, Donangelo R, Lubian J, Hussein M. Recent developments in fusion and direct reactions with weakly bound nuclei. *Phys Rep* (2015) 596:1–86. doi:10.1016/j.physrep.2015.08.001

11. Kolata VJJ, Guimarães AEF. Elastic scattering, fusion, and breakup of light exotic nuclei. *Eur Phys J A* (2016) 123:123. doi:10.1140/epja/i2016-16123-1

12. Keeley N, Alamanos N, Kemper K, Rusek K. Elastic scattering and reactions of light exotic beams. *Prog Part Nucl Phys* (2009) 63:396–447. doi:10.1016/j.ppnp.2009.05.003

13. Ma WH, Wang JS, Mukherjee S, Wang Q, Patel D, Yang YY, et al. Correlation between quarter-point angle and nuclear radius. *Chin Phys C* (2017) 044103:044103. doi:10.1088/1674-1137/41/4/044103

14. Yang Y, Wen PW, Lin CJ, Jia HM, Yang L, Ma NR, et al. Systematic extraction of the strong absorption distance and coulomb barrier from elastic scattering. *Chin Phys C* (2023) 124104:47. doi:10.1088/1674-1137/acf7b8

15. Guimarães V, Cardozo CEN, Lubian J, Assunção M, Pires KCC, Canto LF, et al. Role of cluster configurations in the elastic scattering of light projectiles on Ni and Zn targets: a phenomenological analysis. *Eur Phys J A* (2021) 90:55. doi:10.1140/epja/s10050-021-00403-0

16. Guimarães V, Lubian J, Kolata J, Aguilera EF, Assunção M, Morcelle V. Phenomenological critical interaction distance from elastic scattering measurements on a ^{208}Pb target. *Eur Phys J A* (2018) 223:54. doi:10.1140/epja/i2018-12662-7

17. Pakou A, Rusek K. Interaction distances for weakly bound nuclei at near barrier energies. *Phys Rev C* (2004) 057602:057602. doi:10.1103/PhysRevC.69.057602

18. Benjamim E, Lépine-Szily A, Mendes Junior D, Lichtenthäler R, Guimarães V, Gomes P, et al. Elastic scattering and total reaction cross section for the 6he + 27al system. *Phys Lett B* (2007) 647:30–5. doi:10.1016/j.physletb.2007.01.048

19. Figueira J. M, Niello J. O. F, Abriola D, Arazi A, Capurro O. A, Barbará E. d, et al. Breakup threshold anomaly in the elastic scattering ^{6}Li on ^{27}Al. *Phys Rev C* (2007) 017602:75. doi:10.1103/PhysRevC.75.017602

20. Figueira J. M, Abriola D, Niello J. O. F, Arazi A, Capurro O. A, Barbará E. D, et al. Absence of the threshold anomaly in the elastic scattering of the weakly bound ^{7}Li on ^{27}Al. *Phys Rev C* (2006) 054603:73. doi:10.1103/PhysRevC.73.054603

21. Morcelle V, Lichtenthäler R, Linares R, Morais MC, Guimarães V, Lépine-Szily A, et al. Elastic scattering and total reaction cross section for ^{7}B + ^{27} Al system at near-barrier energies. *Phys Rev C* (2014) 044611:89. doi:10.1103/PhysRevC.89.044611

22. Anjos R, Muri C, Lubian J, Gomes P, Padron I, Alves J, et al. No evidence of break-up effects on the fusion of 9be with medium-light nuclei. *Phys Lett B* (2002) 534:45–51. doi:10.1016/S0370-2693(02)01554-X

23. Morcelle V, Lichtenthäler R, Lépine-Szily A, Guimarães V, Pires KCC, Lubian J, et al. ^{8}B + ^{27} Al scattering at low energies. *Phys Rev C* (2017) 014615:95. doi:10.1103/PhysRevC.95.014615

24. Guimarães V. Fusion cross study from section of 11B + 27Al system (Master degree dissertation - University of Sao Paulo - Brazil). *Instituto de Física* (1988). doi:10.11606/D.43.1988.tde-17062015-061743

25. Hamada S, Burtebayev N, Gridnev KA, Amangeldi N. Further investigation of the elastic scattering of 16o, 14n and 12c on the nucleus of 27al at low energies. *Physica Scripta* (2011) 045201.

26. Mateja J, Stanley D, Theisen L, Frawley A, Pepmiller P, Medsker L, et al. A woods-saxon and double-folding optical-model description of 14n elastic and inelastic scattering from 24mg, 27al and 28si. *Nucl Phys A* (1981) 351:509–18. doi:10.1016/0375-9474(81)90185-8

27. de Faria PN, Lichtenthäler R, Pires KCC, Moro AM, Lépine-Szily A, Guimarães V, et al. Elastic scattering and total reaction cross section of ^{6}He + ^{120}Sn. *Phys Rev C* (2010) 044605:81. doi:10.1103/PhysRevC.81.044605

28. Appannababu S, Lichtenthäler R, Alvarez MAG, Rodríguez-Gallardo M, Lépine-Szily A, Pires KCC, et al. Two-neutron transfer in the ^{6}He + ^{120}Sn reaction. *Phys Rev C* (2019) 014601:99. doi:10.1103/PhysRevC.99.014601

29. Becker K, Blatt K, Jänsch H, Korsch W, Leucker H, Luck W, et al. Polarized 6li scattering from 120sn at 44 mev. *Nucl Phys A* (1991) 535:189–202. doi:10.1016/0375-9474(91)90522-8

30. Chuev V, Glukhov Y, Manko V, Novatskii B, Ogloblin A, Sakuta S, et al. On the interference between coulomb and nuclear excitation in the inelastic scattering of 6li ions. *Phys Lett B* (1972) 42:63–5. doi:10.1016/0370-2693(72)90717-4

31. Zagatto VAB, Lubian J, Gasques LR, Alvarez MAG, Chamon LC, Oliveira JRB, et al. Elastic scattering, inelastic excitation, and neutron transfer for ^{7}Li + ^{120}Sn at energies around the coulomb barrier. *Phys Rev C* (2017) 064614:95. doi:10.1103/PhysRevC.95.064614

32. Arazi A, Casal J, Rodríguez-Gallardo M, Arias JM, Lichtenthäler Filho R, Abriola D, et al. ^{9}Be + ^{120}Snscattering at near-barrier energies within a four-body model. *Phys Rev C* (2018) 044609:97. doi:10.1103/PhysRevC.97.044609

33. Alvarez MAG, Rodríguez-Gallardo M, Gasques LR, Chamon LC, Oliveira JRB, Scarduelli V, et al. Elastic scattering, inelastic excitation, and 1n pick-up transfer cross sections for ^{10}B + ^{120}Sn at energies near the coulomb barrier. *Phys Rev C* (2018) 024621:98. doi:10.1103/PhysRevC.98.024621

34. Gasques LR, Freitas AS, Chamon LC, Oliveira JRB, Medina NH, Scarduelli V, et al. Elastic, inelastic, and 1n transfer cross sections for ^{10}B + ^{120} Sn reaction. *Phys Rev C* (2018) 034629:97. doi:10.1103/PhysRevC.97.034629

35. Acosta L, Álvarez MAG, Andrés MV, Borge MJG, Cortés M, Espino JM, et al. Signature of a strong coupling with the continuum in ^{11}Be+^{120}Sn scattering at the coulomb barrier. *Eur Phys J A* (2009) 42:461–4. doi:10.1140/epja/i2009-10822-6

36. Scarduelli V, Gasques LR, Chamon LC, Zagatto VAB, Alvarez MAG, Lépine-Szily A. Consistent analysis of ^{11}B + ^{120} Sn reaction channels. *Phys Rev C* (2022) 044606:106. doi:10.1103/PhysRevC.106.044606

37. Kundu A, Santra S, Pal A, Chattopadhyay D, Nag TN, Gandhi R, et al. Reaffirmation of probe dependence of the mass deformation length for low-lying excitations ^{112,116,118,120,122,124} Sn isotopes. *Phys Rev C* (2019) 024614:100. doi:10.1103/PhysRevC.100.024614

38. Silva C, Alvarez M, Chamon L, Pereira D, Rao M, Rossi E, Jr, et al. The heavy-ion nuclear potential: determination of a systematic behavior at the region of surface interaction distances. *Nucl Phys A* (2001) 679:287–303. doi:10.1016/S0375-9474(00)00347-X

39. Robertson BC, Sample JT, Goosman DR, Nagatani K, Jones KW. Elastic scattering of ^{16,18} O by ^{116,120} Sn at energies near the coulomb barrier. *Phys Rev C* (1971) 4:2176–80. doi:10.1103/PhysRevC.4.2176

40. Mazzocco M, Keeley N, Boiano A, Boiano C, La Commara M, Manea C, et al. Elastic scattering for the ^{8}B and ^{7}Be + ^{208} Pb systems at near-coulomb barrier energies. *Phys Rev C* (2019) 024602:100. doi:10.1103/PhysRevC.100.024602

41. Linares R, Sinha M, Cardozo EN, Guimarães V, Rogachev GV, Hooker J, et al. Elastic scattering measurements for the ^{10}C + ^{208} Pb system at E_{lab} = 66 mev. *Phys Rev C* (2021) 044613:103. doi:10.1103/PhysRevC.103.044613

42. Magro PLD, Guimarães V, Assunção M, et al. Elastic and inelastic scattering measurements for the 13c+208pb system at close to the coulomb barrier energies. *Eur Phys J A* (2024) 122:60. doi:10.1140/epja/s10050-024-01342-2

43. Távora V, Ovejas J, Martel I, Keeley N, Acosta L, Borge M, et al. Strong coupling effects on near-barrier ^{15}C+^{208}Pb elastic scattering. *Phys Lett B* (2024) 855:138770. doi:10.1016/j.physletb.2024.138770

44. Zerkin V, Pritychenko B. The experimental nuclear reaction data (exfor): extended computer database and web retrieval system. *Nucl Instr Methods Phys Res Section A: Acc Spectrometers, Detectors Associated Equipment* (2018) 888:31–43. doi:10.1016/j.nima.2018.01.045

45. Di Pietro A, Randisi G, Scuderi V, Acosta L, Amorini F, Borge MJG, et al. Elastic scattering and reaction mechanisms of the halo nucleus ^{11}Be around the coulomb barrier. *Phys Rev Lett* (2010) 022701:105. doi:10.1103/PhysRevLett.105.022701

46. Duan FF, Yang YY, Lei J, Wang K, Sun ZY, Pang DY, et al. Elastic scattering and breakup reactions of neutron-rich ^{11}Be on ^{208} Pb at 210 mev. *Phys Rev C* (2022) 034602:105. doi:10.1103/PhysRevC.105.034602

47. Curtis N, Achouri NL, Ashwood NI, Bohlen HG, Catford WN, Clarke NM, et al. Breakup reaction study of the brunnian nucleus ^{10}C. *Phys Rev C* (2008) 021301:77. doi:10.1088/0031-8949/84/04/045201

48. Guimarães V, Cardozo EN, Scarduelli VB, Lubian J, Kolata JJ, O'Malley PD, et al. Strong coupling effect in the elastic scattering of ^{10}C + ^{58} N_i system near barrier. *Phys Rev C* (2019) 034603:100. doi:10.1103/PhysRevC.100.034603

49. Bonaccorso A. Brink DM, Bertulani CA. Proton vs neutron halo breakup. *Phys Rev C* (2004) 024615:69. doi:10.1103/PhysRevC.69.024615

50. Rangel J, Lubian J, Canto LF, Gomes PRS. Effect of Coulomb breakup on the elastic cross section of the ^{8}B proton-halo projectile on a heavy, ^{208}Pb target. *Phys Rev C* (2016) 054610:93. doi:10.1103/PhysRevC.93.054610